Journal of Engineering Science and Technology Review 16 (4) (2023) 133 - 141

Research Article

JOURNAL OF
Engineering Science and Technology Review

www.jestr.org

Micro Forming Studies of SS316L as Biomedical Application Material

Mohit N. Bogar*, Omkar Kulkarni and Ganesh Kakandikar

School of Mechanical Engineering, Dr. Vishwanath Karad MIT World Peace University, Pune, India-411038

Received 22 June 2023; Accepted 2 August 2023

Abstract

The process of shaping flat sheets of metal into necessary shapes without any flaws is known as sheet metal making. Nowadays, there is a growing demand for micro goods and microdevices due to the popularity of miniaturization across many industries. The manufacturing method known as micro forming creates tiny components for various engineering uses. Micro-forming can be found in a variety of fields, including automotive, biomedical, and aerospace engineering. Whenever the sheet material's thickness corresponds to ingrained length distribution of the material being used during the micro-forming process, the deformation behavior is different from what is anticipated for the macroscopic sheet material. A material's ability to be formed is one of the crucial processes, and one of the crucial parameters for determining a material's formability is its forming limit curve or as forming limit diagram. The purpose of this study is plotting Forming Limit Curve for SS316L biomaterial using numerical simulation and experimentation. For the purpose of determining the forming limit curves, a controlled experiment of thin SS316L sheet of 60 µm thickness with different angles in relation to rolling directions (0°, 45°, 90°) is conducted in the present research. In accordance to ASTM-2218-14 standard test, Nakajima test for micro-forming is done using a specimen of uniaxial, uniaxial intermediate, plane, biaxial intermediate and biaxial strain paths to measure limiting strains. The limit diagram for SS316L is formed using the numerical software Simufact Forming V15, and the findings are then compared with the Nakajima test. The comparisons between the experimental method with the numerical simulations show good accordance. To examine the physics of the sheet, micro structural studies are also carried out on the test object both prior to and after forming. It was shown that FLC produced by numerical simulation are designed to be 5% to 12% less than experimental work and are safer. The microstructural study explains the characteristics of the sheet.

Keywords: Micro-forming, Nakajima test, SS316L, FLC, Microstructure.

1. Introduction

Sheet metal forming refers to a procedure that involves applying force onto metallic sheet in order to form into desired shape. While forming process, the sheet may be twisted, stretched, and moulded in a variety of complex forms [1]. A force is applied during this process, causing the material to deform plastically. The sheet may therefore be stretched, bent, or distorted into various kinds of forms. Sheet metal forming is extensively utilized in the aerospace industries, automotive industries, home appliances, biomedical fields and a variety of different industrial domains that demand an accurate forming process [2]. The following Fig. *1* describes some metal forming techniques: deep drawing, stretch forming, shearing, bending, etc.

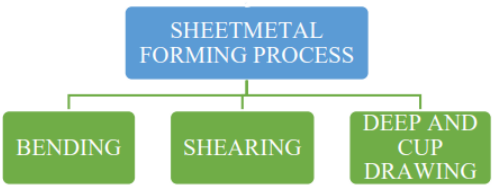

Fig. 1. Sheet Metal Forming Processes

During the forming process, a sheet is compressed through the chamber of the die, that is used to mould metal into shapes like cups. Deep drawing is a metal sheet forming technique in which a sheet metal blank is mechanically pulled radially through a forming die by the action of a punch. As a result, it is a shape modification process with material retention. In this process, a flat metal plate is stretched in some regions to generate a cup shaped hollow or concave shape. The edge of the workpiece is linked to the form, whereupon the punch is forced into the metallic sheet.

The primary goal is understanding the formability of the material chosen, correlating the experimental and numerical investigations and evaluating the microstructural behaviour of the material.

Because of its greater throughput, higher material utilization, and superior characteristics, the micro-forming technique is a viable way of manufacturing micro-parts, particularly in the fields of electronics, energy, and medical applications[3]. The intrinsic length scales of the sheet material used in micro-forming may be on the order of one of the sheet metal's dimensions. Along with other mechanical characteristics of the sheet metal, the forming behaviour will be impacted by these conflicting length scales. The macro forming method and its parameters may not be directly applicable to the micro forming process due to size effects [3].

The effective formability limit of a metal sheet is reflected in its formability. Because metal sheet formability is limited, each material's specific formability should be assessed before

*E-mail address: mohitbogar10@gmail.com
ISSN: 1791-2377
doi:10.25103/jestr.164.17

manufacturing the components. Such a formability constraint prevents the deployment of arbitrary size in the formed portions of the pieces. As a result, a measure must be used to estimate a safe range for deformation values below which no failure will occur[4].

Such a metric may be used to characterise the formability of sheet metal to prevent failure, and it is known as the forming limit diagram (FLD), that includes the safe, critical, and failure zones. The FLD is the most widely used criterion for predicting sheet metal formability and the likelihood of successful or unsuccessful sheet metal forming operations[4]. A key tool for evaluating sheet metal forming is the forming limit diagram (FLD) or forming limit curve (FLC). A graphical depiction of major strain as well as minor strain at each point on a component is a forming limit diagram. As shown in Figure 2, the green dots represent the strains for the forming curve while the red line curve depicts the strain paths in the forming curve.

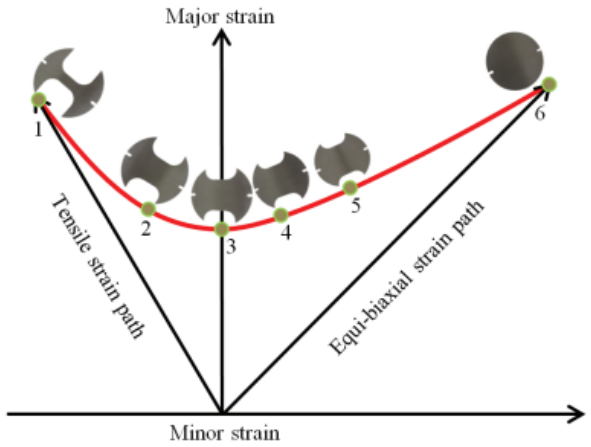

Fig. 2. Schematic diagram of FLC[5]

Analytical, numerical, and experimental are the methods which can be used to plot the limit curves. Sheet metal has a very narrow thickness range of 0.1 to 5 mm, with the majority of sheets used for forming operations having a thickness of less than 1.5 mm; hence, surface strain has a significant influence on strain measurement. Surface strain measuring is a challenging challenge as well. To identify surface strain, several grid patterns are put on the sheet[6]. Because of its simplicity, grid marking is one of the most routinely used strain measurement methods for strain analysis in sheet metal forming operations. The method of grid marking involves printing line patterns at the desired location on a blank of sheet metal.[7] In the experimental technique, a grid of tiny circles with a centre-to-centre spacing in the same range and a diameter of 1 or 2 millimetres are printed on a blank surface. The circle will be transformed into ellipses depending on strain routes throughout the formation process. Major and minor strains may be estimated from these ellipses, and if surface strains are known, thickness can be determined using the volume constancy principle [1]. The out of plane experiment (e.g., Nakajima test), during which a sheet metal sample is secured within circular dies and stretched using a hemispherical punch, is one of the most renowned tests to achieve the FLD experimentally. Under all the deformation paths, it is discovered that as the punch diameter increases it leads to the increase in the failure plastic strain. Also, the failure plastic strain reduces as the deformation speed increases[8]. The region of potential necking failure (unsafe zone) is shown by the FLD as a curve across the critical combination of the major and minor strains of a component which is undergoing deformation. Different strain ratios, from uniaxial compression to equibiaxial tension, would be plotted on the FLD. [4].

When the feature size of a component is decreased to less than 1mm, a phenomenon known as size effect occurs, causing traditional forming process knowledge in regards to empirical as well as analytical know-how to be inapplicable in the micro-forming environment. Many efforts have been made to demonstrate that material behaviour at the micro-scale differs to the macro-scale[9]. Hence, the aim of this study is to perform experiments at micro level i.e., 60 microns thickness. There are three types of scale effects: density-based, shape-based, and texture-based. Micro-friction, the size of the grain, the orientation, its thickness, tool geometry, the spring back effect, the coarse grain effect, and many other factors influence these final two categories.[10]. The material's grain size has a significant impact on the material's formability. More or larger grain size, means reduced formability. The material's ideal grain size, which is between 10 and 11 µm, exhibits higher formability attribute. When a material with a larger grain size is deformed dislocations move more easily than when a material with a lower grain size is deformed. Because less force is required and there are fewer grains, larger grain-size materials fail much faster than smaller grain-size materials[9]. All materials' measurements of grain size demonstrate that the grain size is about in the same region. A metallographic microscope is utilized for identifying faults in metal surfaces as well as to assess grain boundaries, grain size, and phase analysis.

This study intends to demonstrate the capacity of Bio-material Stainless Steel (SS316L) to develop using one of the inquiry methodologies, FLC. In the current study, the thickness of the biomaterial employed is 60 µm.

In this research, forming limit curves were drawn using the ASTM-2218-14 Limiting Dome Height Test[11]. The specimens used are uni-axial, uni-axial intermediate, plane, bi-axial intermediate and bi-axial strain pathways. Micro forming experimental setup is devised and developed. Limit dome height tests on 60 µm thin SS316L sheet were done for three distinct orientations for rolling directions (0°, 45°, and 90°). In comparison to rolling directions of 45° and 90°, thin foil with a 0° rolling direction provides a higher safe zone. Foil has the smallest safe zone when rolling in a 90° direction [12]. All three orientations were chosen to investigate the influence of rolling direction upon formability. In a similar way the procedure has been numerically simulated using Simufact Forming software and limit curves have been formed for three distinct orientations for rolling directions (0°, 45°, and 90°).

2. Materials and Methodology

For industrial micro forming applications, knowing the process's limiting factors is crucial. The unique properties of the micro formation may be connected to the limiting factors[13], [14].

Size effects are well known to play a vital part in micro forming techniques, as well. When handling microscale parts or work-pieces, several unanticipated alterations happen as a result of size effects. Investigations and evaluations of each material utilised in any microform-related process, especially microstamping, must be regarded as crucial to fully understand their behaviour and relate it to the process [15], [16].

To investigate the influence of foil thickness on the forming behaviour of SS316L austenitic stainless steel, economically feasible foil about thickness of 60 µm was employed. Table 1 shows the chemical composition of this material.

The human body uses biomaterials in many different places, including hip and knee joints, Oro dental structures, artificial heart valves, artificial shoulders replacement implants, and artificial knee and elbow joints[17].

Particularly titanium alloys, Co-Cr alloys, along with stainless steel alloys are frequently used as materials for orthopaedic implants. Due to its superior resistance to corrosion, good mechanical qualities, ease of fabrication, and low cost in comparison to titanium alloys, stainless steel 316L has emerged as one of those most frequently utilised biomaterials in the implementation of implants[18], [19].

SS-316L has a higher molybdenum concentration compared with other chromium-nickel austenitic stainless-steel alloys, which enhances corrosion resistance. 316L stainless steel has long been a popular alloy in most implant sectors, including cardiovascular, dental, orthopaedic, and otorhinolaryngology. Because of its ability in replacing the functions of hard tissues, it is suited in bone fixation process like plate, screw as well as artificial joints in the orthopaedic sector. It consists of electronics, pharmaceuticals, automobiles, medical implants such as pins, screws, and orthopaedic implants as like the replacements in hips and knees. The higher the percentage of Cr, the better the corrosion resistance and as a result, this material is well suited for use in the biomedical industry.

Also, for the chosen material at thickness 60 µm, research work is yet to be done. Secondly, the thickness 60 µm is selected as for biomedical materials such as SS316L, forming limit curves are not available for thin foils below 100 µm. It has been noted that in all research, the formability and forming processes were examined on a macro scale i.e., more than 100 µm.

Table 1. Chemical Composition of SS316L

Element	Fe	Cr	Ni	Mo	Si	Mn	Co	P	S	C
Content (% wt.)	67.690	16.630	10.850	2.00	1.28	0.38	0.21	0.045	0.03	0.018

2.1 Specimen Preparation

Screen printing was used to create SS316L specimens with a circular grid, as illustrated in Figure 4. The circular grids are printed straightaway on the metallic sheet with help of suitable ink resistant to the process of metal forming in this approach[20]. The thus produced circle measures 01 mm in diameter, and there is a 02 mm center-to-center distance between adjacent circles. During micro forming, those circles are going to deform to an elliptical shape; deformations are monitored in the main and minor axis directions for plotting the FLC [21]. The sheet is then cut into the desired forms making use of Wire-Cut EDM in accordance with the ASTM E2218-14 standard. WEDM is a very precise technique that results in excellent precision and a high level of surface polish[22]. The machine method aids in lowering the material's overall stress concentration [23]. Because the specimen is already small, any other method of obtaining the form will result in a stress concentration region at some point [24],[25]. If there is a concentration of tension in one location, the results achieved will be impeded; hence, this procedure is applied [26]. Figure 3 depicts the tensile specimens cut by WEDM in mentioned rolling orientations.

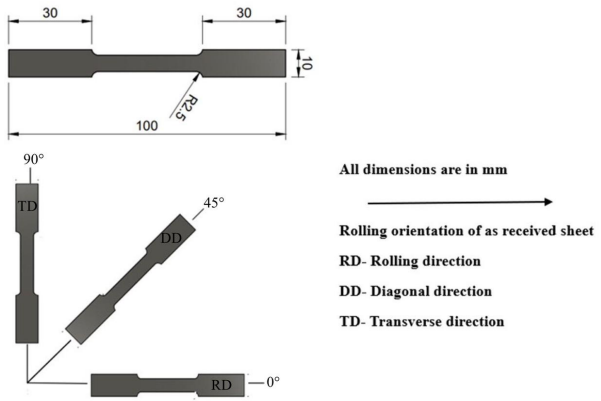

Fig. 3. Tensile specimens in Rolling directions (0°,45°,90°)

Throughout the rolling process, the material experiences plastic deformation, which causes the grain structure to start elongating in the rolling direction. The rolled material's mechanical properties are anisotropic as a result of this occurrence, with higher stiffness along the rolling direction than the transverse direction. The anisotropy is thus defined in relation to rolling direction as r' = $\frac{r_0+2r_{45}+r_{90}}{4}$[21]. Where, r_0, r_{45}, r_{90} are the rolling directions.

Three of the six produced specimens provide uniaxial strain paths, plane strain paths, and biaxial strain paths, while the rest of three provide intermediate paths within them. The total diameter of all the specimens is 10mm. The samples in the current research are produced in accordance with the Nakajima test, as demonstrated in Figure 5.

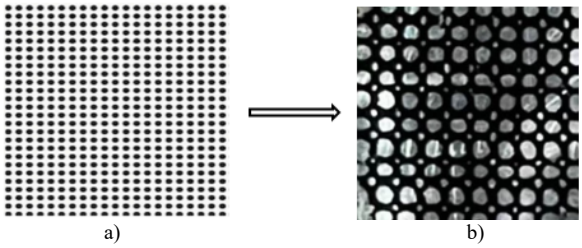

Fig. 4. Circular grid preparation on specimen SS316L [21] a) Circular grids of 1mm diameter and b) Circular grids printed on sheet

2.2 Experimental Investigation

Experimentation began with the design and assembly of a tool setup [27] [28]. The tool is made up of two die sets, one upper and one lower, with a cavity in between to provide the pressure plates to be fitted into and room for the blank. This tool is uniquely constructed with a hemispherical punch with a diameter of 4mm and a diameter of 4.5mm in the die sets. Bolts are utilized to fasten the connection of top and bottom dies. The pressure plates are used for holding of blank in place. The blank is sandwiched among the pressure plates and the dies. To execute the Nakajima test, the entire tooling setup is installed onto the Universal Testing Machine (UTM) with a 5.0 KN capability. Figure 6 depicts this tool configuration. During the studies, the crosshead speed is 2mm/min.

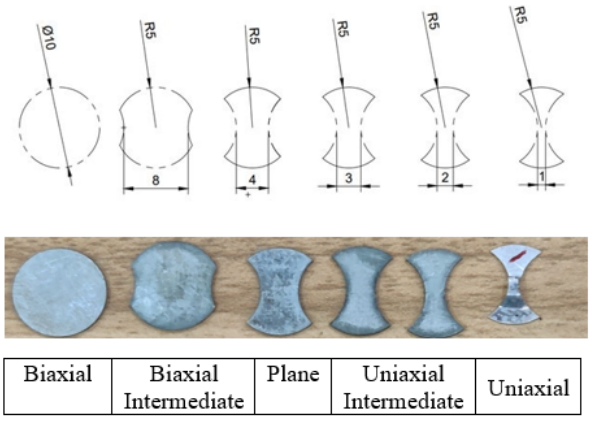

Fig. 5. Specimen preparation: ASTM E2218-14 standard

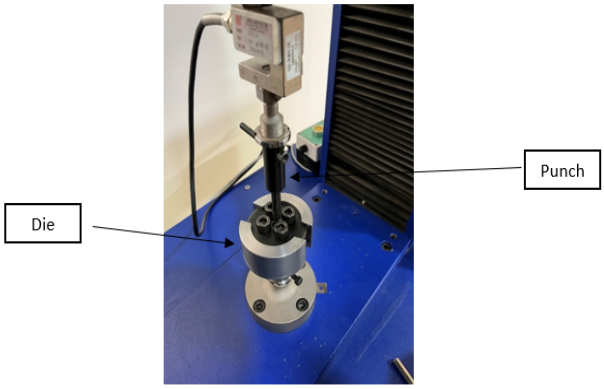

Fig. 6. Experimental tool configuration

Six distinct specimens were subjected to the ASTM 2218-14 norm, often known as the Nakajima experiment. As shown in Fig. 3, the specimens used for the experiment had already been screen-printed with a circular grid. During deformation phase, each specimen is moved towards the creation of a single fracture. In this procedure, three trials for all six specimens of each rolling direction were carried out. The average value of the major and minor strains of three trials is taken. To boost the accuracy, major and minor stresses were measured wherever the fracture was evident using a vision measuring device. The measurements were taken precisely where the necking had happened. Minor strains were anticipated by evaluating minor axis nearby necking area, while major strains were anticipated by evaluating major axis. Major along with minor strains were established using a simple formula that defines strain as a ratio of length change to original length. This aids in the representation of the FLC of the material. The experiment concluded in each of the six strain paths, as seen in Figure 7. The specimen's dome structure has a minor crack, which clearly shows ductile failure.

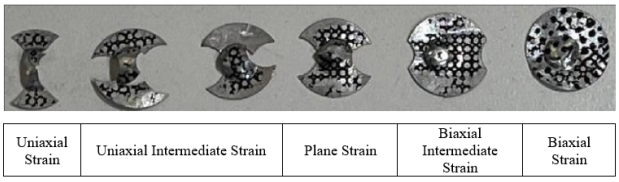

Fig. 7. Formed Samples after Nakajima Test for all strain paths

2.3 Tensile Test

A tensile test truly necessary to document the material's characteristics. The tensile test results provide information about the material's properties that includes its tensile strength, elongation %, yield stress, also the peak load. This information needs to be provided for inputs for the simulation software to do the numerical analysis. The tensile test specimen is developed in accordance with the ASTM standard E8/E8M − 13a [29] showed in Figure 8.

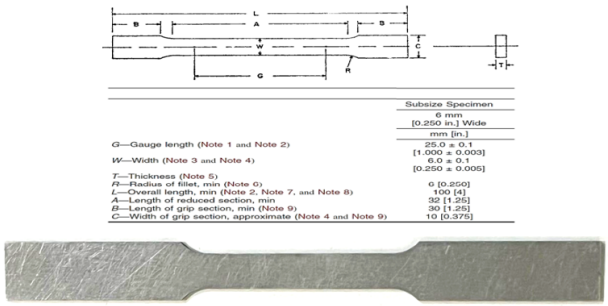

Fig. 8. Standard Tensile Test Specimen as per ASTM standard E8/E8M − 13a [29]

To decrease stress concentration, WEDM is utilized to prepare specimen for the tensile test. This test was performed on a 5.0 KN UTM machine equipped with a custom fixture developed for holding the specimen. The tensile test was performed over constant velocity of 9 mm/min. Fig9 depicts the tensile test conduct of a 60 µm SS316L thin foil. The material's mechanical properties were determined by the test's conclusion.

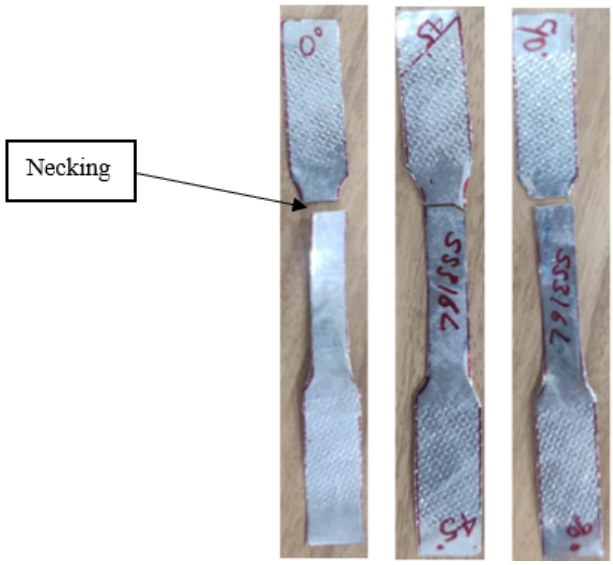

Fig. 9. Tensile Test on SS316L thin foil

2.4 Numerical Investigation

A numerical simulation of strain distribution and blank dimensions can be helpful in making a precise prediction of deformation. Through the use of finite element analysis, numerical platforms have become the most used tools. This will provide process insight without requiring immediate testing.

2.4.1 CAD Modelling

In the CAD software, models of the tool itself and blank are created. Autodesk Fusion 360 software was used in the CAD design of the punch, die and the specimens used for the experimental work. Fig10 shows the CAD model of the tool setup used for simulation.

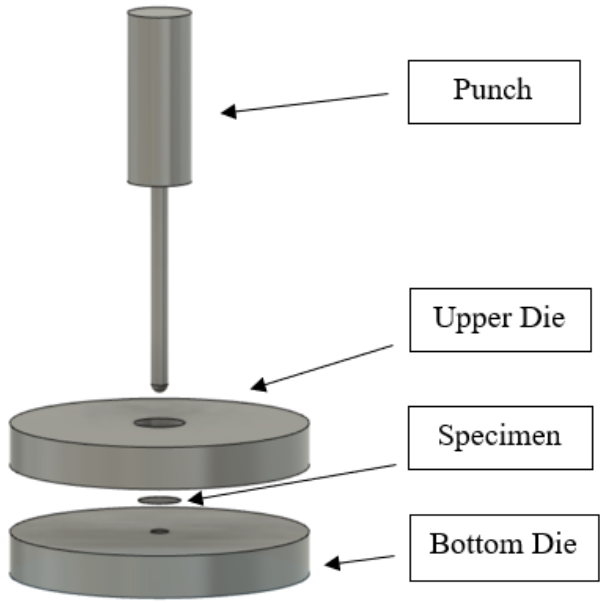

Fig. 10. CAD model of tool setup

2.4.2 Finite Element Modelling

Using a pre-processor, boundary conditions have been described plus documented in an information database. The boundary conditions used are symmetry lines or clipped edges. Plastic strains have been taken into account since plastic deformation is always present during forming. The ductile damage criteria were applied. The material parameters and data supplied to the software, including density, yield stress, Poisson's ratio and FLD damage criterion, were imported through the tensile test. As a result, in this study, Simufact Forming software was used for the numerical simulation. Simulated strain paths include bi-axial, bi-axial intermediate, plain, uniaxial intermediate 1, uniaxial intermediate 2 and uniaxial. Simufact Forming's database has a wide range of materials. New user-defined materials, on the other hand, may be provided to the database. Here, both major and minor strains were taken into consideration as outcomes. Fig. 11 displays the FE model of the tool for simulation of Biaxial strain path in 0° rolling direction.

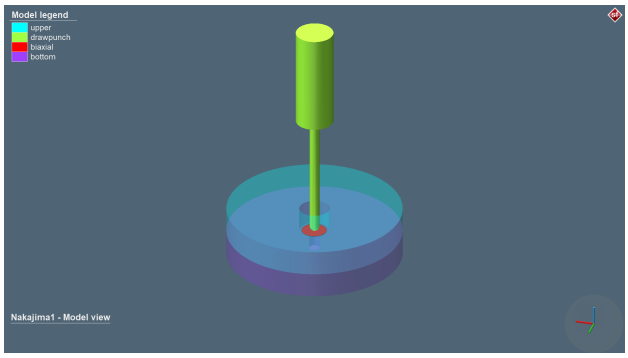

Fig. 11. FE model of tool setup for Biaxial strain path in 0° rolling direction

The Nakajima test parameters for the Biaxial strain path in 0° rolling direction are presented in Table 2.

Table 2. Test Parameters for Nakajima Test Simulation

Hemispherical Punch Diameter	**4.00 mm**
Bottom Die Inner Diameter	4.25 mm
Biaxial Specimen Material	SS316L
Biaxial Specimen Thickness	0.06 mm
Velocity of Punch	2 mm/min
Stroke for Punch	1.62 mm
Friction Coefficient	0.1
Element Type	Hexahedral Sheetmesh
Element Size of Blank	2 mm
Rolling Direction of Specimen	0°

Likewise, the FE models of the other strain paths in all three distinct rolling directions (0°, 45°, 90°) were created and the boundary conditions, material properties of the strain path specimens, mechanical properties and required information were used for the numerical simulation in Simufact Forming software.

3 Results and Discussions

All six specimens had their strain paths examined, and a vision measuring tool was utilized to evaluate the major as well as minor strains. Each specimen establishes a location on the graph that finally provides the material's FLC. During the Nakajima test, the specimen was transformed into a dome shape, and onsite necking was observed.

Figure 12 shows how circular dots on the specimens were turned into ellipses at necking. The most crucial areas for determining limiting strains are the circles at the fracture zone. Surface strain has been measured using the lengths of the major and minor axes of ellipses. An optical microscope was used to take the readings.

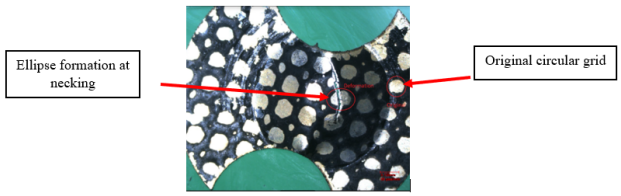

Fig. 12. Deformed Sample

Equations (1) and (2) are applied in order to compute the specimen's major as well as minor strain.

$$Major\ strain = \frac{major\ axis\ length - original\ circle\ diameter}{original\ circle\ diameter} * 100 \quad (1)$$

$$Minor\ strain = \frac{minor\ axis\ length - original\ circle\ diamter}{original\ circle\ diameter} * 100 \quad (2)$$

3.1 Experimental Results

The primary goal of experimenting is to produce and plot limit curves. Forming limit curves was developed based on testing for desired thickness and varied rolling directions. The region underlying the forming limit curve is regarded the safer zone for a certain thickness technique of forming, whereas the area over its forming limit curve is referred to the failure zone. Table 3 displays the values of all six strain paths of 60 µm SS316L sheet in three distinct directions of rolling (0°, 45°, 90°) at the position of the crack in the sample. Figure 13 depicts the FLC plotted for experimental procedure of all strain paths in different rolling directions (0°, 45°, 90°). It has been shown that failure limit curves for higher major strains are produced by orientation about 0° to the rolling direction.

Table 3. Experimental measurement of strain paths

Rolling Direction	Specimen	Minor Strain	Major Strain
0°	Uniaxial	-0.1479	0.4713
	Uniaxial Intermediate I	-0.0970	0.3265
	Uniaxial Intermediate II	-0.0692	0.2173
	Plane	0.00459	0.1409
	Biaxial Intermediate	0.1113	0.3685
	Biaxial	0.1707	0.4692
45°	Uniaxial	-0.1257	0.4644
	Uniaxial Intermediate I	-0.082	0.3065
	Uniaxial Intermediate II	-0.054	0.1623
	Plane	0.00469	0.1099
	Biaxial Intermediate	0.1116	0.3385
	Biaxial	0.1711	0.4429
90°	Uniaxial	-0.1235	0.4774
	Uniaxial Intermediate I	-0.092	0.3061
	Uniaxial Intermediate II	-0.0589	0.1573
	Plane	0.00437	0.0809
	Biaxial Intermediate	0.1064	0.3285
	Biaxial	0.1693	0.4809

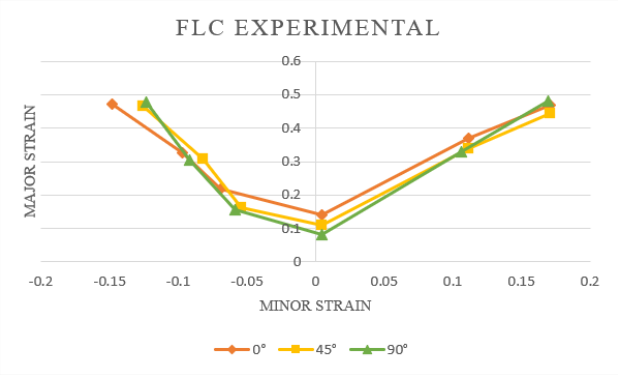

Fig. 13. Forming Limit Curve by Experimental method of SS316L

From the above experimental results for all the three rolling directions, it has been observed that, for the SS316L foil, 0° rolling direction has higher safer zone compared to the 45° and 90° directions. The foil with 90° direction has the least safe zone.

3.2 Numerical Results

Figure 14 shows both major and minor strains accounting of all strain paths according to each of the rolling directions (0°, 45°, 90°) for a 60 µm foil specimen.

The results are depicted in Table 4. This data has been used to generate limit curves. Figure 15 depicts the FLC plotted for numerical simulation of all strain paths in different rolling directions (0°, 45°, 90°).

Table 4. Numerical Simulation measurements of six strain paths

Rolling Direction	Sample Type	Minor Strain	Major Strain
0°	Uniaxial	-0.1338	0.4407
	Uniaxial Intermediate I	-0.0931	0.3068
	Uniaxial Intermediate II	-0.0663	0.2006
	Plane	0.00441	0.1231
	Biaxial Intermediate	0.1042	0.3345
	Biaxial	0.1574	0.4490
45°	Uniaxial	-0.11513	0.4379
	Uniaxial Intermediate I	-0.0750	0.2884
	Uniaxial Intermediate II	-0.0580	0.1811
	Plane	0.00454	0.0979
	Biaxial Intermediate	0.1011	0.3178
	Biaxial	0.1521	0.4296
90°	Uniaxial	-0.1121	0.4362
	Uniaxial Intermediate I	-0.0911	0.281
	Uniaxial Intermediate II	-0.0622	0.1455
	Plane	0.00427	0.0767
	Biaxial Intermediate	0.0995	0.3142
	Biaxial	0.1574	0.4511

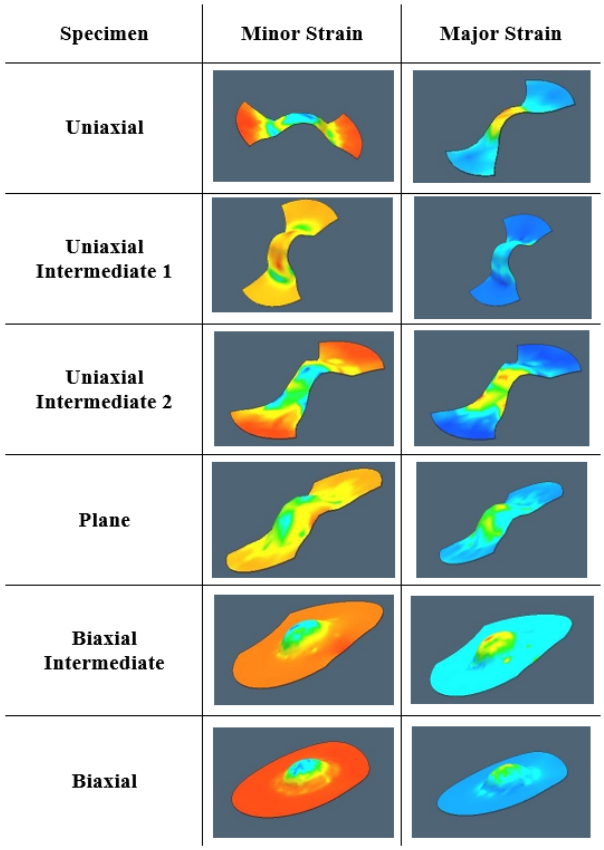

Fig. 14. Major and Minor Strains for all strain paths

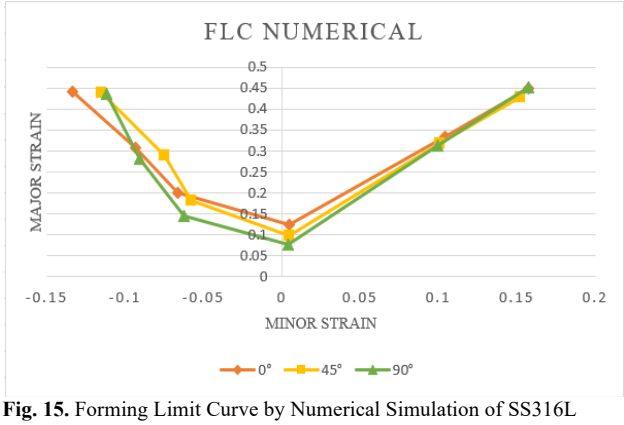

Fig. 15. Forming Limit Curve by Numerical Simulation of SS316L

The numerical simulation findings for all three rolling directions show that the 0° rolling direction has a larger safety zone than the 45° and 90° directions for the SS316L foil. The foil with a 90° angle has the smallest safe zone.

3.3 Microstructural Study

An optical microscope was used to analyse the microstructure. It is required to prepare the specimens before

utilising optic and scanning electron microscopy. Wire cut machining process in the defined rolling directions was used to cut the samples. The samples' surfaces were polished afterwards utilizing a Selvyt cloth for lapping and colloidal silica gel after their grinding with fine paper of an 800-grit size. Lastly, electrolytic etching was performed by immersing in a 10% oxalic acid dissolved in a H_2O solution for 30 seconds at 15 Volts for the optical microscope observation. The microstructural image of SS316L specimen is shown in Figure 16.

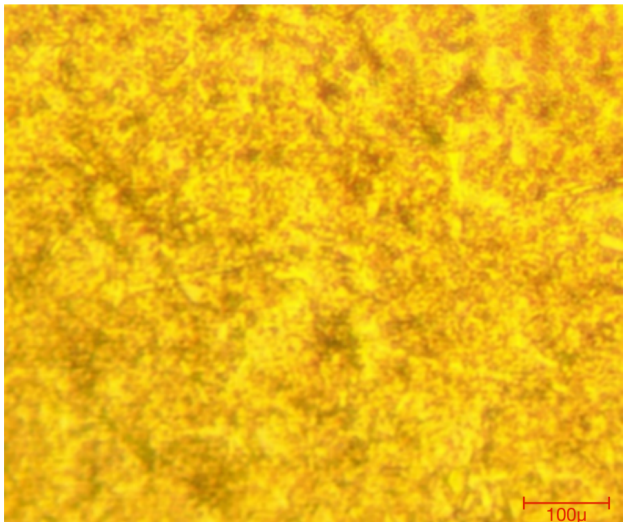

Fig. 16. Microstructural image of SS316L

The measurement of grain sizes and phase analysis are carried out using image analysis software, as illustrated in Table 5 and Table 6. The granular size of SS316L was examined according to ASTM - E 112-13/E 1382-97 standard, which measured 10.24 µm.

Table 5. Grain size measurement of SS316L

Parameter	Value
ASTM Grain Size	10.24
Single Field Area	0.82 mm^2
No. of Fields	1

Table 6. Phase analysis of SS316L

Parameter	Value
Austenite (γ)	79.65%
Delta – Ferrite (δ)	20.35%

The phase analysis was done in compliance to the ASTM - E562-11 standard, and it was discovered that austenite (γ) and delta-ferrite (δ) phases have been identified in the microstructure, with austenite accounting for 79.65 % & delta-ferrite accounting for 20.35 %.

Based on the microstructural analysis carried out, it can be stated that that a material's strength is lower when its grain size is larger than it is when it is smaller. And as a result, reduces the formability of the material. In this research, the average grain size is found to be 10.24 µm which is an ideal value which lies within the range of 10-11 µm.

4 Comparison of both methods

The following Fig. 17, Fig. 18 and Fig. 19 for a 60 µm sheet show how the two techniques compare to one another. It is clear that the numerical technique produces results that are almost identical to the experimental data.

In experimental work, the plane strain for 60 µm with 0° rolling direction was determined to be 0.1409, whereas the numerical technique found it to be 0.1231. This demonstrates that the FLC obtained through the experimental technique is greater than the FLC obtained using the numerical simulation method. Numerical FLC appears to be lower for SS316L, ensuring a safer design. The experimental area provides a safer region.

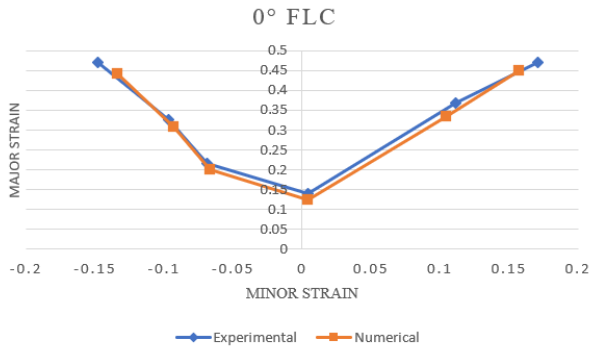

Fig. 17. Comparison of FLC: Experimental and Numerical

During experimental work, the plane strain for 60 µm sheet with 45° rolling direction was determined to be 0.1099, whereas the numerical technique found it to be 0.0979. This demonstrates that the FLC obtained through the experimental technique is greater than the FLC obtained using the numerical method. Numerical FLC appears to be lower for SS316L, ensuring a safer design. The experimental area provides a safer region.

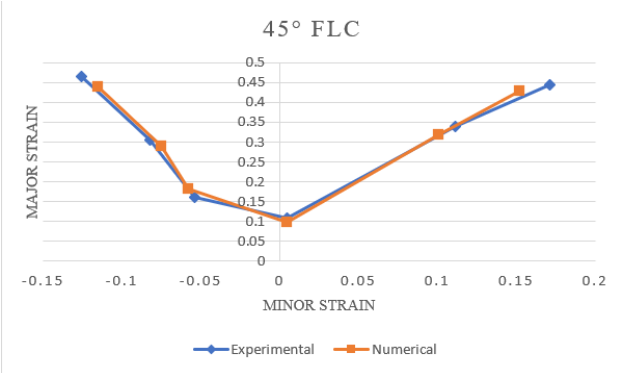

Fig. 18. Comparison of FLC: Experimental and Numerical

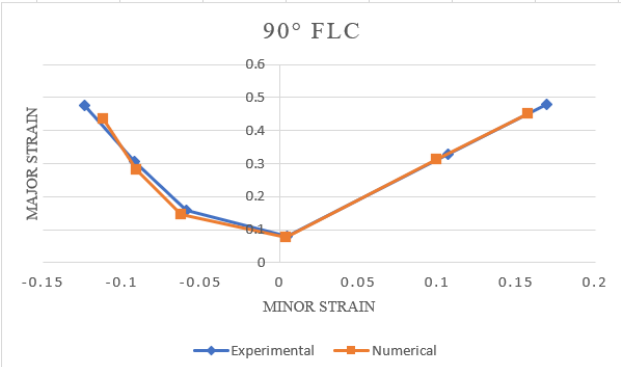

Fig. 19. Comparison of FLC: Experimental and Numerical

In experimental work, the plane strain for 60 µm with 90° rolling direction was determined to be 0.0809, whereas the

numerical technique found it to be 0.0767. This demonstrates that the FLC obtained through the experimental technique is greater than the FLC obtained using the numerical simulation method. Numerical FLC appears to be lower for SS316L, ensuring a safer design. The experimental area provides a safer region.

5 Conclusions

The paper covers the micro-forming procedure, the forming limit diagram, and the SS316L material employed. The material SS316L is employed in several biomedical fields. Using an experimental and numerical technique, forming limit curves are drawn. Experimental research employed the hemispherical punch test. The experiment is carried out in three distinct rolling directions. To determine the mechanical characteristics of the material that is to be used in the simulation, a tensile test is conducted on the material. Simufact Forming is used for the numerical simulation. Comparative of FLC from simulation and experimental work is carried out. Utilizing an optical microscope, microstructural analysis is observed to understand the behaviour of the material. The behaviour of the material is further studied using grain size analysis as well as phase analysis. To better understand the behaviour of formability, materials are subjected to microstructural investigation. It has been effectively proven that the experimental work for the behaviour of ductile damage and deformations has a high safer region. It is possible to conclude from experimental method as well as numerical simulation of SS316L thin foil sheet that,

1. Using six distinct strain paths, the FLCs for the micro-forming behaviour of SS316L are effectively plotted. This broadens our understanding of the forming process.
2. The SS316L foil with a 0° rolling direction offers a larger safe zone than the foil with a 45° or 90° rolling direction.
3. The numerical simulation model for modelling deformations and ductile damage behaviour has been effectively put together.
4. The comparable behaviour of the Forming Limit Curves displayed numerically and experimentally shows that the numerical model created provides extensive insight into the physical aspects of the process.
5. By plotting FLD, this study sets a significant standard that will aid researchers in part design & micro forming manufacturing, notably regarding biomedical applications as well as other uses of SS316L.
6. Study has been done on the microstructure analysis for the micro forming and the grain size, phase analysis has been evaluated.

As a result of the foregoing conclusions, it is clear that having a material with the suitable composition is crucial for producing a high strength. In order to develop an implant material with the best possible qualities, it is important to thoroughly understand how each element affects phase transformation and the resulting microstructure.

List of Abbreviations

µm	Micro Meter
ASTM	American Society for Testing and Materials
CAD	Computer Aided Drawing
Co-Cr	Cobalt-Chromium
FE	Finite Element
FLC	Forming Limit Curve
FLD	Forming Limit Diagram
kN	Kilo Newton
SS316L	Stainless Steel 316L
UTM	Universal Testing Machine
WEDM	Wire Cut Electric Discharge Machine

Acknowledgements

The authors would like to thank and acknowledge the support offered by the professors of Mechanical Engineering, Faculty of Engineering & Technology, Dr. Vishwanath Karad's MIT World Peace University, for their contribution to the review paper.

References

[1] G. Patel, K. Ganesh M., and O. Kulkarni, "Experimental and numerical investigations on forming limit curves in micro forming," *Adv. Mat. Process. Technol.*, vol. 8, no. 1, pp. 33–44, Jan. 2022, doi: 10.1080/2374068X.2020.1793268.

[2] S. D. Kumar, T. R. Amjith, and C. Anjaneyulu, "Forming Limit Diagram Generation of Aluminum Alloy AA2014 Using Nakazima Test Simulation Tool," *Proc. Technol.*, vol. 24, pp. 386–393, 2016, doi: 10.1016/j.protcy.2016.05.053.

[3] J. Sahu, S. Chakrabarty, R. Raghavan, and S. Mishra, "Investigations of size effect on formability and microstructure evolution in SS304 thin foils," *J Str Anal Eng Des*, vol. 53, no. 7, pp. 517–528, Oct. 2018, doi: 10.1177/0309324718792443.

[4] M. H. Sehhat, A. Mahdianikhotbesara, and M. Hadad, "Forming Limit Diagrams of Perforated St12 Steel Sheets," In Review, preprint, Oct. 2021. doi: 10.21203/rs.3.rs-1025499/v1.

[5] Z. Shao *et al.*, "Experimental investigation of forming limit curves and deformation features in warm forming of an aluminium alloy," *Proc Inst Mech Eng B J Eng Manuf*, vol. 232, no. 3, pp. 465–474, Feb. 2018, doi: 10.1177/0954405416645776.

[6] P. Wankhede and K. Suresh, "A review on the evaluation of formability in sheet metal forming," *Advances in Materials and Processing Technologies*, vol. 6, no. 2. Taylor and Francis Ltd., pp. 402–429, Apr. 02, 2020. doi: 10.1080/2374068X.2020.1731229.

[7] K. Hariharan and C. Balaji, "Material optimization: A case study using sheet metal-forming analysis," *J Mater Process Technol*, vol. 209, no. 1, pp. 324–331, Jan. 2009, doi: 10.1016/j.jmatprotec.2008.01.063.

[8] C. Sudarsan, K. H. Banker, S. Hazra, R. Bhagat, and S. K. Panda, "Experimental investigations on forming limit diagram of ultra-thin SS 304 steel: effect of circular grid size, sheet orientation, punch size and deformation speed," *Adv Mat Process Technol*, vol. 5, no. 1, pp. 25–38, Jan. 2019, doi: 10.1080/2374068X.2018.1510679.

[9] M. A. Musa, A. R. Razali, and N. I. Kasim, "Grain and Feature Size Effect on Material Behavior for Micro-Sheet-Forming," *AMM*, vol. 680, pp. 77–80, Oct. 2014, doi: 10.4028/www.scientific.net/AMM.680.77.

[10] C. Pradeep Raja and T. Ramesh, "Influence of size effects and its key issues during microforming and its associated processes – A review," *Eng Sci Technol Int J*, vol. 24, no. 2, pp. 556–570, Apr. 2021, doi: 10.1016/j.jestch.2020.08.007.

[11] E28 Committee, "Test Method for Determining Forming Limit Curves," ASTM International. doi: 10.1520/E2218-14.

[12] G. Patel and G. Kakandikar, "Investigations on effect of thickness and rolling direction of thin metal foil on forming limit curves in microforming process," in *Mod Manuf Process* Elsevier, 2020, pp. 145–155. doi: 10.1016/B978-0-12-819496-6.00007-5.

[13] N. Tiwari, G. Kakandikar, and O. Kulkarni, "Micro Forming and its Application: A Critical Review," *J. Eng. Res. & Sci.*, vol. 1, no. 3, pp. 126–132, Mar. 2022, doi: 10.55708/js0103013.

[14] P. Pesode, S. Barve, Y. Mane, S. Dayane, S. Kolekar, and K. A. Mohammed, "Recent Advances on Biocompatible coating on Magnesium alloys by Micro Arc Oxidation Technique," *KEM*, vol. 944, pp. 117–134, Apr. 2023, doi: 10.4028/p-p8yk47.

[15] J. H. Deng, M. W. Fu, and W. L. Chan, "Size effect on material surface deformation behavior in micro-forming process," *Mater Sci Eng A*, vol. 528, no. 13–14, pp. 4799–4806, May 2011, doi: 10.1016/j.msea.2011.03.005.

[16] V. Kohale, S. Jawade, and G. Kakandikar, "Investigation on mechanical behaviour of inconel 718 manufactured through additive manufacturing," *Int J Interact Des Manuf*, vol. 17, no. 4, pp. 1645–1651, Aug. 2023, doi: 10.1007/s12008-022-01183-7.

[17] M. Geetha, A. K. Singh, R. Asokamani, and A. K. Gogia, "Ti based biomaterials, the ultimate choice for orthopaedic implants - A review," *Prog in Mater Sci* vol. 54, no. 3. pp. 397–425, May 2009. doi: 10.1016/j.pmatsci.2008.06.004.

[18] D. Singh, R. Singh, K. S. Boparai, I. Farina, L. Feo, and A. K. Verma, "In-vitro studies of SS 316 L biomedical implants prepared by FDM, vapor smoothing and investment casting," *Compos B Eng*, vol. 132, pp. 107–114, Jan. 2018, doi: 10.1016/j.compositesb.2017.08.019.

[19] P. Pesode and S. Barve, "A review—metastable β titanium alloy for biomedical applications," *J. Eng. Appl. Sci.*, vol. 70, no. 1, p. 25, Dec. 2023, doi: 10.1186/s44147-023-00196-7.

[20] E. Carasusan and F. Canal, "An automated procedure for non-contact strain analysis of sheet metal parts," in *EFTA 2003. 2003 IEEE Conference on Emerging Technologies and Factory Automation. Proceedings (Cat. No.03TH8696)*, Lisbon, Portugal: IEEE, 2003, pp. 724–731. doi: 10.1109/ETFA.2003.1248770.

[21] A. Mashalkar, G. Kakandikar, and V. Nandedkar, "Micro-forming analysis of ultra-thin brass foil," *Materials and Manufacturing Processes*, vol. 34, no. 13, pp. 1509–1515, Oct. 2019, doi: 10.1080/10426914.2019.1655158.

[22] K. Natarajan *et al.*, "Study on Optimization of WEDM Process Parameters on Stainless Steel," *J Nanomat*, vol. 2022, pp. 1–7, Jul. 2022, doi: 10.1155/2022/6765721.

[23] P. S. Gowthaman and S. Jeyakumar, "A Study on Wire Electrical Discharge Machining Process Parameters and Performances," in *Adv Mater Manufac Eng*, T. Rajmohan, K. Palanikumar, and J. P. Davim, Eds., in Springer Proceedings in Materials, vol. 7. Singapore: Springer Singapore, 2021, pp. 195–201. doi: 10.1007/978-981-15-6267-9_23.

[24] T. R. Ablyaz, E. S. Shlykov, K. R. Muratov, and S. S. Sidhu, "Analysis of Wire-Cut Electro Discharge Machining of Polymer Composite Materials," *Micromachines*, vol. 12, no. 5, p. 571, May 2021, doi: 10.3390/mi12050571.

[25] C. G. Burande, O. K. Kulkarni, S. Jawade, and G. M. Kakandikar, "Process parameters optimization by bat inspired algorithm of CNC turning on EN8 steel for prediction of surface roughness," *J Mechatr Artif Intellig Eng*, vol. 2, no. 2, pp. 73–85, Dec. 2021, doi: 10.21595/jmai.2021.22148.

[26] M. M. Kane, A. A. Phanse, H. J. Bahirat, and S. V. Kulkarni, "Classification and comparative study of EDM pulse generators," *IET P Electr*, vol. 13, no. 14, pp. 3146–3154, Nov. 2020, doi: 10.1049/iet-pel.2020.0205.

[27] O. Kulkarni and G. Kakandikar, "Novel product design of tool for investigating formability with microstructural study of bio-material titanium grade-II thin foils," *Int J Interact Des Manuf*, Jun. 2022, doi: 10.1007/s12008-022-00903-3.

[28] O. Kulkarni and G. Kakandikar, "Formability Assessment with Microstructural Investigations for Zirconium 702 Thin Foils: Bio-Material Applications," *Adv Mat Process Technol*, vol. 8, no. sup4, pp. 2367–2377, Nov. 2022, doi: 10.1080/2374068X.2022.2044131.

[29] E28 Committee, "Test Methods for Tension Testing of Metallic Materials," ASTM International. doi: 10.1520/E0008_E0008M-13A